

What Hinders Perceptual Quality of PSNR-oriented Methods?

Tianshuo Xu^{1*}, Peng Mi^{1*}, Xiawu Zheng¹, Lijiang Li¹, Fei Chao^{1†}, Guannan Jiang², Wei Zhang², Yiyi Zhou¹, Rongrong Ji¹

¹Media Analytics and Computing Lab (MAC), School of Informatics, Xiamen University

²Intelligent Manufacturing Department, Contemporary Amperex Technology Co. Limited (CATL)

{xutianshuo, mipeng, zhengxiawu, lilijiang}@stu.xmu.edu.cn

{fchao, zhouyiyi, rrji}@xmu.edu.cn, {jianggn, zhangwei}@catl.com

Abstract

PSNR-oriented models (POMs) have achieved great success and are widely adopted in many image super-resolution (SR) applications. However, details of images generated by these models are usually over-smoothed. Many existing methods improve the perceptual quality of generated images by designing models with larger sizes to optimize the models' learning ability, or using GAN-based models to generate fake details. Unfortunately, those methods cost too much labor effort to be practical in real-world applications. To solve this issue, in this paper, we discover two factors that inhibit POMs from achieving high perceptual quality: 1) center-oriented optimization (COO) problem and 2) model's low-frequency tendency. First, POMs tend to generate an SR image whose position in the feature space is closest to the distribution center of all potential high-resolution (HR) images, resulting in such POMs losing high-frequency details. Second, 90% area of an image consists of low-frequency signals; in contrast, human perception relies on an image's high-frequency details. However, POMs apply the same calculation to process different-frequency areas, so that POMs tend to restore the low-frequency regions. Based on these two factors, we propose a Detail Enhanced Contrastive Loss (DECLoss), by combining a high-frequency enhancement module and spatial contrastive learning module, to reduce the influence of the COO problem and low-Frequency tendency. Experimental results show the efficiency and effectiveness when applying DECLoss on several regular SR models. E.g., in EDSR, our proposed method achieves $3.60\times$ faster learning speed compared to a GAN-based method with a subtle degradation in visual quality. In addition, our final results show that an SR network equipped with our DECLoss generates more realistic and visually pleasing textures compared to state-of-the-art methods.

*Both authors contributed equally to this research.

†Corresponding author.

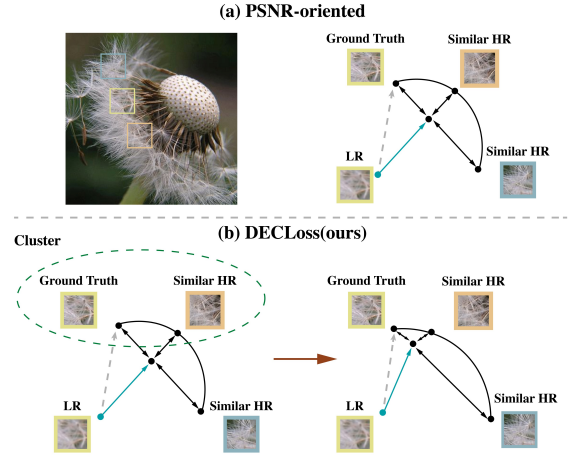


Figure 1. Schematic diagram of the COO problem. The gray dotted arrow denotes the correct mapping, and green arrow denotes the actual mapping under the COO problem. After applying our DECLoss, LR is divided into specific groups for more accurate mapping, so as to reduce this problem's influences.

1. Introduction

Image super-resolution (SR) aims to construct a high-resolution (HR) image from its low-resolution (LR) counterpart. SR is an important class of image processing and has been widely applied on real-world tasks [6, 12, 27, 39]. With the rapid development of deep learning, deep neuron networks have shown promising performance in SR [5, 14, 17, 19, 36]. Many of them pre-defined SR as a pixel-level mapping from LR-to-SR and adopted MAE/MSE loss to pursue high Peak Signal to Noise Ratio (PSNR), such models are termed as PSNR-oriented models (POMs).

Existing methods [19, 36] prefer to crop input LR images to patches during training, e.g., 192×192 . However, in these cropping processes, these LR patches lost contextual information and high-frequency details during down-

Mean average error and mean square error, respectively.

sampling operations. Such a phenomenon increases the probability that two regions are similar in their LR form, but the two regions are not identical before down-sampling. If the similarity of these two LR regions exceeds the model’s discriminative ability, the model must be optimized to map these two regions to a distribution center of their HR regions in the feature space (Fig. 1(a)). Thus, these generated HR images contain very similar low-frequency signals (this is why their LR regions are similar), but their image details are different. As a result, these generated images are over-smoothed. We name such a phenomenon as “the center-oriented optimization (COO) problem”, hindering POMs from producing clear-detail images.

In addition, Piatykh *et al.* revealed that the key to human perception of image quality is the high-frequency information [26]. In contrast, POMs used MAE/MSE loss functions to assign the same calculation for areas with different frequencies; however, low-frequency-oriented regions of an image are over 90%. This situation drives POMs to tend to restore the low-frequency regions. Two mainstream types of existing approaches aimed at improving the perceptual quality of generated images, *w.r.t.* creating larger models or using GAN-based methods, to both indirectly weaken the COO problem and reduce the low-frequency tendency. In particular, larger-size models improved the upper bound of the discriminate ability, thus achieving accurate mappings from LR to HR. GAN-based methods generated fake details, whose distribution is close to details of the real-world HRs. However, both methods led to more calculations and latency. Moreover, GAN-based methods are unstable and time-consuming during training.

In this paper, we propose a Detail Enhanced Contrastive Loss (DECLoss) for SR networks to alleviate the COO problem and eliminate the low-frequency tendency. The main idea of DECLoss is to precisely map an LR region to an HR region, even if the HR region is not the LR’s ground truth. DECLoss consists of two calculation steps 1) high-frequency enhancement and 2) spatial contrastive learning. To cope with human perception, we first enhance image details by compensating the high-frequency information in the Fourier domain. We then reshape the SR patches and their corresponding HR patches to a sequence of mini-patches. For each SR mini-patch, within a training batch, we select all HR mini-patches that are really similar to the SR’s ground truth as positive samples, and rest HR mini-patches are negative samples. Next, we introduce contrastive learning to reduce the distance of positive samples and increase that of negative samples. Therefore, the SR model can accurately map each different region of LR to an HR region, so as to augment the details of the generated image (Fig. 1(b)). It is the first time that we have combined contrastive learning with region similarity in SR. Without any adversarial operations, our DECLoss is stable and straightforward.

In summary, our main contributions are three-fold:

1) Revealing Obstructions for High Perceptual Quality.

We reveal the factors hindering POMs from generating high perceptual quality images, *w.r.t.* the center-oriented optimization problem and low-frequency tendency. In particular, it is the first time that we define the COO problem and quantify effects of this problem on SR models.

2) Proposing a Detail Enhanced Contrastive Loss (DECLoss).

We propose a novel perceptual-driven loss function. Based on the image frequency transformation and contrastive learning, DECLoss alleviates the COO problem and eliminate the low-frequency tendency, to achieve the higher perceptual quality.

3) Extensive Experiments.

Extensive experiments demonstrate the efficiency and effectiveness of our methods. Without any adversarial operations, our DECLoss, *e.g.*, in EDSR [19], our DECLoss based method achieves equivalent performance with a GAN-based method with $3.60\times$ faster; and combined with RaGAN [36], our RRDB [36] model outperform a variety of state-of-the-art methods.

2. Related Work

2.1. Image Super-Resolution

Image super-resolution is an important image restoration task in computer vision [8, 21, 23, 29–31]. Since SRCNN [5] first applied early convolutional neural networks to solve SR tasks. VDSR [14] also used a very deep network for SR. When He *et al.* [10] proposed ResNet for learning residuals, SRResNet [17] introduced ResBlock [10] to expand the network depth. EDSR [19] further enhanced the efficiency of residual methods to advance SR results. DRCN [15], DRRN [32], and CARN [2] also adopted ResBlock [10] for the recursive learning. Then, RRDB [36] and RDN [43] used dense connections to augment information from former layers. RCAN [42] and RFA [20] explored an attention mechanism within a deep SR model.

To improve the perceptual quality and append missing details caused by the COO problem. Johnson *et al.* [13] proposed a perceptual loss; and Zhang *et al.* [40] proposed a training-based model, “LPIPS”, to measure perceptual distances of images. SRGAN [17] first introduced a GAN-based method into an SR model, where an adversarial loss was used during training. ESRGAN [36] made a significant progress for GAN-based methods. Images generated by ESRGAN looked more natural in texture. In contrast, Beby-GAN [18] paid more attention to generating fake details, thereby further improving the perceptual quality. In particular, their research on the over-smoothed phenomenon of SR inspired us to discover of COO problem. Although GAN-based methods are effective in generating fake details, due to the two-stage gradient backpropagations and system

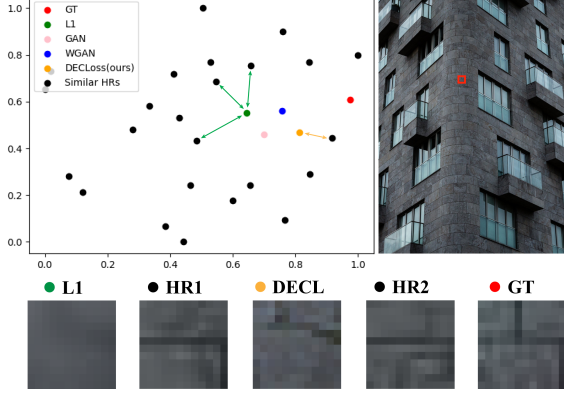


Figure 2. Visualized tiny detail regions by t-SNE [33]. HR1 and HR2 are similar HRs of ground truth (GT), L1 is trained by 1-norm loss, and DECLoss is our proposed metric loss. Influenced by COO problem, L_1 node is mapped to the center of adjacent HRs. In particular, DECLoss is closer to an HR node in perceptual perspective.

I/O, GAN-based methods cost too much in training.

2.2. Contrastive Learning

Contrastive Learning demonstrates its effectiveness in unsupervised representation learning [7, 25, 35] tasks. The contrastive learning method is to learn representations, which similar samples stay close to each other, while dissimilar samples are far apart [3, 4, 9]. Many super-resolution approaches also applied contrastive learning to improve their robustness. E.g., DASR [34] applied contrastive learning in the degradation representations. Wang *et al.* [37] proposed a distillation method with contrastive learning. Zhang *et al.* [38] used a bidirectional contrastive loss to identify both high-frequency and low-frequency features.

3. Center-Oriented Optimization Problem

Center-oriented optimization (COO) problem is: when dealing with several hard-to-discriminate LR inputs, POMs tend to map an LR input to the distribution center of all potential HR, resulting in generating over-smoothed outputs, shown in Fig. 2. Therefore, we first describe in mathematics that how the COO problem influences the quality of POMs. Therefore, a function must be established to describe the influences of the COO problem.

3.1. Problem Description

POMs usually pre-define the super-resolution as an LR input x mapping to an HR image \hat{y} through a function G_θ , so as to make \hat{y} be as similar as possible to the ground truth y . Thus, we have:

$$\hat{y} = G_\theta(x). \quad (1)$$

Input/output, this paper mainly refers to the tensors.

Then, to minimize the distance $d(\cdot)$ between an SR image \hat{y} and its corresponding ground truth y , the function G_θ updates its parameter θ by using:

$$\hat{\theta} = \arg \min_{\theta} \sum_{i=1}^N d(\hat{y}_i, y_i). \quad (2)$$

However, in the real world, a region x_i from an LR image might be very similar to another LR region x_j that model $G_{\hat{\theta}}(x)$ cannot discriminate; however, x_i, x_j 's corresponding HR (y_i, y_j) are different in details. Then, we have:

$$\hat{y}^* = G_{\hat{\theta}}(x_i) = G_{\hat{\theta}}(x_j), \quad (3)$$

$$D = d(\hat{y}^*, y_i) + d(\hat{y}^*, y_j), \quad (4)$$

where D denotes the summarized distance of two similar SR patches (\hat{y}^*, \hat{y}^*) with their ground truth (y_i, y_j). Therefore, the model $G_{\hat{\theta}}$ is forced to optimize the distance, so that SR \hat{y}^* must be close to the center of HRs (y_i, y_j):

$$\min(D) = d\left(\frac{y_i + y_j}{2}, y_i\right) + d\left(\frac{y_i + y_j}{2}, y_j\right), \quad (5)$$

$$\hat{y}^* = \arg \min_{\hat{y}^*} (D) = \frac{y_i + y_j}{2}. \quad (6)$$

We then extend Eq. 6 to the entire data set:

$$\hat{y}^*(x) = \frac{1}{N} \sum_{i=1}^N \sigma(x, y_i) y_i, \text{ s.t. } \sum_{i=1}^N \sigma(x, y_i) = 1, \quad (7)$$

where $\sigma(\cdot)$ is the mapping probability from LR x to HR y_i . For example, if LRs are not similar to each other, thus, an example mapping probability is [0.97, 0.02, 0.01]; however, if LRs are similar to each other, their probability is [0.4, 0.4, 0.2]. Unfortunately, it is difficult to calculate these probabilities.

Note that, the image down-sampling loses the high-frequency information, *i.e.*, HRs usually look the same at the low-frequency regions but their high-frequency details are different. Therefore, the details of generated images are blurry; however, these high-frequency details are very important to the perceptual quality.

3.2. Description Function

Due to the difficulties in calculating the probabilities defined in Eq. 7, we analyze how to measure the intensity of the COO problem (ICOO) by using feature distances. Therefore, we first assume that each LR image x is well mapped to its corresponding HR image y by the function G_θ . The distance $d(\cdot)$ between each SR \hat{y}_i with corresponding HR y_i is approximately zero and the distance from other HR y_j are positive; thus we have:

$$\hat{y} = G_\theta(x), \quad d(y, \hat{y}) \rightarrow 0, \quad (8)$$

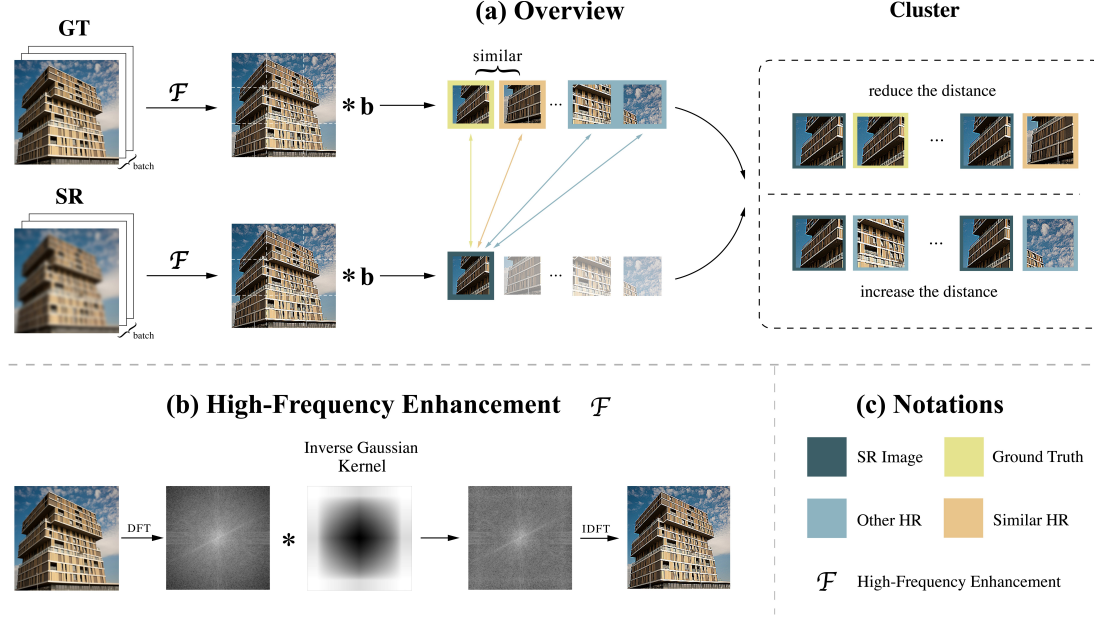


Figure 3. The overview of DEC Loss. (a) We first apply the high-frequency enhancement to eliminate the Low-Frequency Tendency. Within a training batch, we then reshape the enhanced image into a sequence of flattened mini-patches. Eventually, we cluster the mini-patches to polarize the details, which reduce the influence of the COO problem. (b) The details of the high frequency enhancement process via Eq. 12-Eq. 16. (c) The relevant notations.

$$P(\hat{y}_i) = \frac{d(y_i, \hat{y}_i)}{\sum_{j=1}^N \mathbb{1}_{[j \neq i]} d(y_j, \hat{y}_i)} \rightarrow 0, \quad (9)$$

where $P(\hat{y})$ denotes the mapping accuracy of SR \hat{y} ; N denotes the length of a dataset, or, N can also denote the top- k similar HR images of SR \hat{y} . It is possible to relax the condition of Eq. 9, so that SR \hat{y}_i can reach any potential HR y_j , even if the HR is not the ground truth y_i . Since the clarity of image detail is the key to human perception of image quality [26], the mapping accuracy of image details is usually not essential. Thus, Eq. 9 is rewritten as:

$$P^*(\hat{y}_i) = \frac{d(y_k, \hat{y}_i)}{\sum_{j=1}^N \mathbb{1}_{[j \neq k]} d(y_j, \hat{y}_i)}, \quad (10)$$

where y_k denotes the HR image with the shortest distance from \hat{y}_i . Then, we can describe the intensity of the COO problem $S(G_{\hat{\theta}})$ through the sum of the score defined in Eq. 10 with multiple generated images \hat{y} :

$$\begin{aligned} S(G_{\hat{\theta}}) &= -10 \times \log_{10} \left(\sum_{i=1}^M P^*(\hat{y}_i) \right) \\ &= -10 \times \log_{10} \left(\sum_{i=1}^M \frac{d(y_k, \hat{y}_i)}{\sum_{j=1}^N \mathbb{1}_{[j \neq k]} d(y_j, \hat{y}_i)} \right), \end{aligned} \quad (11)$$

where M denotes the length of a proper subset of a dataset; and we use the logarithm function to avoid too small values.

Eq. 11 is the core function to reflect the intensity of the COO problem (ICOO). Note that, ICOO measures similarities between SR and HR distributions, rather than to measure two image’s similarity. Such distribution similarities represent the overall SR image quality. The ICOO measurement is described in Sec. 5.2.

4. Method

Detail enhanced contrastive loss (DEC Loss) is a novel loss function of SR, which aims to alleviate the COO problem and eliminate the Low-Frequency Tendency, so as to increase the perceptual quality of SR images.

4.1. Overview

DEC Loss is regarded as a perceptual-driven loss function for image SR. DEC Loss does not require any generate-adversarial processes, which are not efficient and effective. Fig. 3 shows that DEC Loss consists of two steps – the high-frequency enhancement and spatial contrastive loss, optimized for the Low-Frequency Tendency and COO problem, respectively. First, We enhance details of SR images and their HR images (\hat{y}, y), paying more attention to the high-frequency regions, which are more fit to the human perception [26]. Second, we reshape the both SR images and HR images into a sequence of mini-patches. DEC Loss with a smaller patch size is more sensitive in feature similarities, so that it can improves the clustering results. Finally, we

introduce the “contrastive learning” to cluster mini-patches according to their corresponding HR similarities. Note that, reducing the distance of similar SR images solves the limitation that POMs can only map LR to their ground truth. In addition, enlarging the distance of different groups also increases the difficulty in mapping an LR to the distribution center of similar HRs (Eq. 6).

4.2. High-Frequency Enhancement

In order to increase high-frequency details of POMs, we enhance the image’s high-frequency in Fourier space. As illustrated in Fig. 3(b), we first use the Discrete Fourier Transform (DFT) F to map a SR image \hat{y} and its ground truth y (denoted as Y), to the Fourier domain Y_f :

$$Y_f = F^{(H)} Y F^{(W)}, \quad (12)$$

where H and W are the height and width of an image Y , respectively; and each component of $F^{(H)}$ is defined as:

$$F_{jk}^{(N)} = \exp(-2\pi i j k / N), \quad i = \sqrt{-1}. \quad (13)$$

We then multiply the inverse Gaussian kernel vector K with the Fourier matrix to obtain:

$$Y'_f = \left(K^{(H)}\right)^T K^{(W)} \cdot Y_f, \quad (14)$$

where each component of $K^{(H)}$ is defined as:

$$K_i^{(N)} = \alpha \times \exp\left(\frac{-(i - (N - 1)/2)^2}{2 \times \mu^2}\right), \quad (15)$$

where α and μ are control variables. Finally, we use the Inverse Discrete Fourier Transform (IDFT) F^* to map the Fourier matrix Y'_f back to the image domain Y^* :

$$Y^* = \frac{1}{HW} \left(F^{(H)}\right)^* Y'_f \left(F^{(W)}\right)^*, \quad (16)$$

where $F^{(N)}$ is defined as:

$$\left(F^{(N)}\right)^* = \left(\text{real}\left(F^{(N)}\right) - \text{imag}\left(F^{(N)}\right)\right)^T, \quad (17)$$

where $\text{real}(\cdot)$ and $\text{imag}(\cdot)$ are the real part and imaginary part of a complex number, respectively. Note that, the inverse Gaussian kernel provides a smooth importance for regions in different frequencies, suppresses the low-frequencies, and enhances the high-frequencies, so as to alleviate the Low-Frequency Tendency.

4.3. Spatial Contrastive Loss

The spatial contrastive loss is regarded as the key method alleviating the COO problem. Based on similarities of HRs, we control the mapping range of COO problem by using

contrastive clustering. Fig. 3(a) illustrates that we first reshape the high-frequency enhanced (Sec. 4.2) input patches $Y^* \in \mathbb{R}^{B \times C \times H \times W}$ into a sequence of flattened 2D mini-patches $Y^{*p} \in \mathbb{R}^{(B \times N) \times C \times P \times P}$, where (H, W) is the resolution of the original patch, C is the number of channels, B is the batch size, (P, P) is the resolution of each mini-patch, and $N = HW/P^2$ is the resulting number of mini-patches. Similarly, a mini-patch is more polarized than a normal patch, which is more beneficial for subsequent clustering operations.

We initially measure the cosine similarities of each SR-to-HR $S^{sr \rightarrow hr}$, and SR-to-SR $S^{sr \rightarrow sr}$:

$$S_{ij}^{sr \rightarrow hr} = \frac{\hat{y}_i^{*p} \hat{y}_j^{*p}}{|\hat{y}_i^{*p}| |\hat{y}_j^{*p}|}, \quad S^{sr \rightarrow hr} \in \mathbb{R}^{B^* \times B^*}, \quad (18)$$

$$S_{ij}^{sr \rightarrow sr} = \frac{\hat{y}_i^{*p} \hat{y}_j^{*p}}{|\hat{y}_i^{*p}| |\hat{y}_j^{*p}|}, \quad S^{sr \rightarrow sr} \in \mathbb{R}^{B^* \times B^*}, \quad (19)$$

where $B^* = B \times N$ is the number of a batch of HR mini-patches. To better discriminate the positive samples and negative samples, we regard the PSNR similarities of HR-to-HR as a mask $M \in \mathbb{R}^{B^* \times B^*}$:

$$M_{ij} = -20 \times \log_{10}\left(\frac{\|y_i^{*p} - y_j^{*p}\|_2}{\text{MAX}}\right), \quad (20)$$

where $*$ denotes high-frequency enhanced (Sec. 4.2), p denotes mini-patch, $\|\cdot\|_2$ is the L_2 -norm, and MAX is the upper bound of color space. In particular, if the similarity M_{ij} is greater than a threshold η , the input is regarded as a positive sample; otherwise, it is a negative sample. Then, the scores of the positive samples Q_{pos} and negative ones Q_{neg} are represented as:

$$Q_{pos,i} = \sum_{j=1}^{B^*} \mathbb{1}_{[M_{ij} > \eta]} (e^{S_{ij}^{sr \rightarrow sr}} + 2e^{S_{ij}^{sr \rightarrow hr}}) / t_{pos}, \quad (21)$$

$$Q_{neg,i} = \sum_{j=1}^{B^*} \mathbb{1}_{[M_{ij} < \eta]} (e^{S_{ij}^{sr \rightarrow sr}} + 2e^{S_{ij}^{sr \rightarrow hr}}) / t_{neg}, \quad (22)$$

where t_{pos}, t_{neg} are temperatures. Note that $2 \times e^{S^{sr \rightarrow hr}}$ is equivalent to the original contrastive learning matrix [4]. DECLoss L_d is defined as:

$$L_d = -\frac{1}{B^*} \sum_{i=1}^{B^*} \log\left(\frac{Q_{pos,i}}{Q_{neg,i}}\right). \quad (23)$$

4.4. Loss Function

Inspired by the Perceptual Loss [13], we apply the L_1 and perceptual loss L_p in our model. L_1 loss is the 1-norm distance between a generated image and its ground truth,

Table 1. Ablation study results. We compare different configurations of loss functions. Red font denotes the best and blue denotes the second best. We calculate restoration metrics PSNR, perceptual metric LPIPS [40] and our proposed COO strength metric Eq. 11. Config., denotes different loss configurations, ICOO is the our proposed metric (Eq. 11) to measure the intensity of the COO problem, and GPU Hs., represents the GPU hours required for a complete training. RaGAN is the GAN metric of ESRGAN [36]. All metrics are calculated on the DIV2K [1] validation set.

Config.	Model	L1	VGG [13]	DECLoss	GAN [17]	RaGAN [36]	↑ PSNR	↓ LPIPS	↓ ICOO	↓ GPU Hs.
1	EDSR	✓					28.56	0.273	28.54	6.33
2	EDSR	✓		✓			27.22	0.179	28.23	6.61
3	EDSR	✓	✓				26.44	0.166	26.60	8.94
4	EDSR	✓	✓		✓		26.34	0.160	26.42	33.56
5	EDSR	✓	✓			✓	26.25	0.157	26.15	34.22
6	EDSR	✓	✓	✓			26.71	0.160	26.73	9.50
7	EDSR	✓	✓	✓		✓	26.36	0.153	25.90	33.89
8	RRDB	✓	✓	✓			28.47	0.118	26.75	43.22
9	RRDB	✓	✓			✓	26.64	0.092	25.58	67.72
10	RRDB	✓	✓	✓		✓	27.01	0.090	25.83	71.08

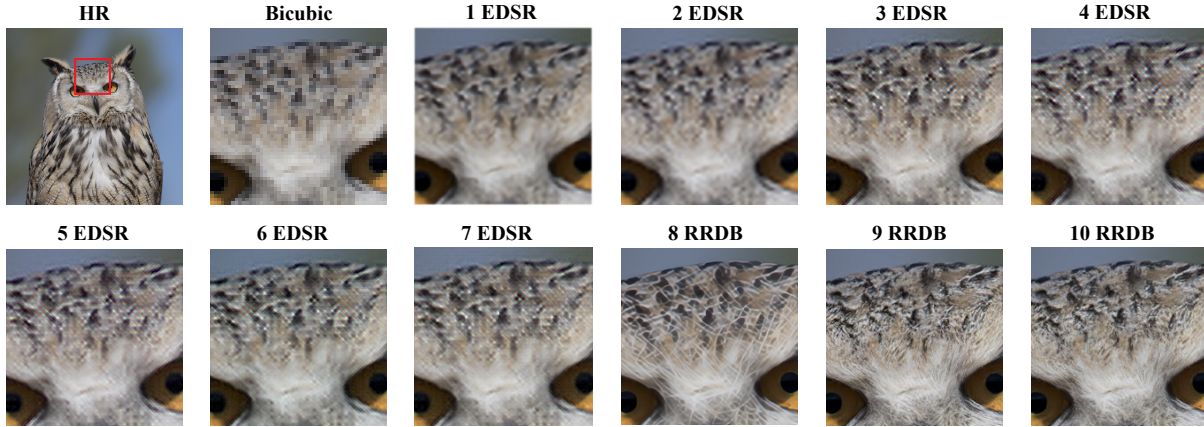


Figure 4. Comparison of different configurations of losses. The image is the 0880.png of DIV2K [1]. The models correspond to the table above. Our proposed DECLoss has higher perceptual quality and richer realistic details.

which ensures the image reconstruction quality. Thus, L_1 loss is defined as:

$$L_1 = \sum_{i=1}^N \|\hat{y} - y\|_1. \quad (24)$$

The perceptual loss measures the distance in the feature space. We specify a pre-trained VGG-19 [28] to generate the feature map, denoted as φ :

$$L_p = \sum_{i=1}^N \|\varphi(\hat{y}) - \varphi(y)\|_2. \quad (25)$$

The total loss function L is defined as:

$$L = \omega_1 \times L_1 + \omega_2 \times L_p + \omega_3 \times L_d, \quad (26)$$

where ω_1 , ω_2 , and ω_3 are the weights to balance different loss terms.

5. Experimentation

5.1. Settings

We train all the models on DIV2K [1] dataset that consists of 2,000 resolution 800 training images, 100 validation images, and 100 test images. To obtain training LR data, we down-sample the HR images using the bicubic interpolation. We evaluate all models on famous SR benchmarks: DIV2K(test) [1], BSD100 [24], and Urban100 [11]. We mainly produce experiments on EDSR and RRDB models. By following [19], all experiments are performed with a scaling factor of $\times 4$ between LR and HR images. Then, we crop patches with size 48×48 and size 192×192 from LR and HR, respectively. To ensure the fairness of comparisons, the batch size of all models is set to 32. There are 1,000 batches in each training round.

We divide the training process into two stages. First, we pre-train all the models with L_1 loss (Eq. 24) as an initial-

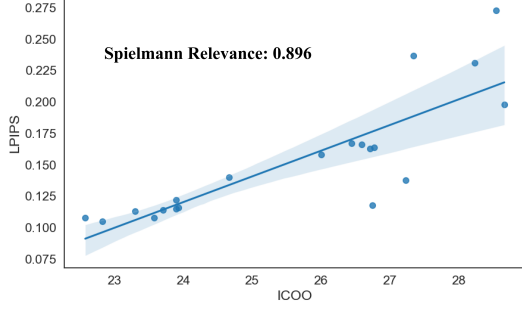


Figure 5. Relationships between ICOO and LPIPS scores on Urban100 [11].

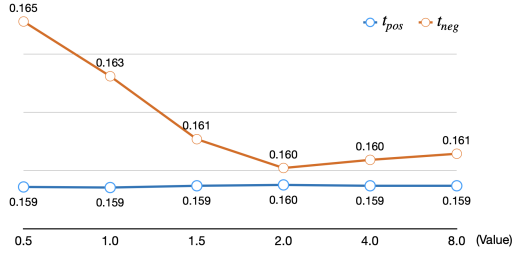


Figure 6. Comparisons of different temperatures. The blue curve represents the LPIPS variation of t_{pos} , and red curve represents t_{neg} .

ization, with 200 epochs, and 5 warm-up epochs. We use a cosine learning rate with $\gamma = 0.5$ and its initial learning rate is set to 1×10^{-4} . This pre-training with L_1 loss helps the model converge to a certain range. Second, the generator is trained using the loss function defined in Eq. 26 with $\omega_1 = 1 \times 10^{-2}$, $\omega_2 = 1$, $\omega_3 = 3 \times 10^{-5}$. The temperature (t_{pos}, t_{neg}) is set to (0.5, 1.5). Due to the trade-off between number of mini-patches and computation resource, the size of mini-patch is 8×8 . The learning rate is set to 2×10^{-5} and cosine learning rate is applied to a decay schedule. For the optimization, we use the Adam algorithm [16] with $\beta_1 = 0.9$ and $\beta_2 = 0.999$. We implement our models with PyTorch and train on $4 \times$ A100 GPUs.

5.2. Intensity of COO Problem

We proposed a function to measure the intensity of the COO problem (Eq. 11), termed ICOO. ICOO calculates distribution similarities between SRs and HRs, rather than measuring two image’s similarities. The mini-patch size is 12×12 , $N = 8$ and $M = 100$; these parameters indicate that eight SR mini-patches are randomly cropped for each SR, and 100 HR mini-patches are cropped for each HR. We test ten rounds to average the results, so as to reduce influences of the randomness. Fig. 5 shows that we randomly selected and trained 20 models on Urban100 [11], with various architectures and initialization. The Spielman Relevance

score of ICOO with LPIPS is 0.892, demonstrating a high positive correlation between ICOO and LPIPS. We also added our ICOO metrics in the comparison.

5.3. Ablation

Comparison of different loss configurations. We conducted an ablation study with different loss configurations to exhibit the effectiveness of our DECLoss. In Table 1 and Fig. 4, Config. 1 indicates results of the basic EDSR; Config. 2 represents results of the DECLoss with restoration loss L_1 ; Config. 3 represents results of the perceptual loss; Configs. 4, 5, and 9 are results of the GAN metric Losses; Configs. 6 and 8 present results of our DECLoss trained with perceptual loss [36]. In Configs. 2 and 6, the results of our DECLoss outperformed those of Configs. 1 and 3, respectively. Config. 6 also has the equivalent performance with those of the GAN-based metrics: Configs. 4 and 6. Also, results of Config. 8 achieve similar scores with those of Config. 9. We also conduct the orthogonality of DECLoss that train with RaGAN [36] in Configs. 7 and 10; the results in LPIPS of Configs. 7 and 10 are lower than 0.004 and 0.002 of Configs. 5 and 9, respectively.

Influence of contrastive temperatures. Following original contrastive learning [4], we introduced two temperature values to balance the intensity of both positive and negative samples. As shown in Fig. 6, we tested the performance of $t_{pos} = [0.5, 1.0, 1.5, 2.0, 4.0, 8.0]$ with a fixed $t_{neg} = 1.5$. We then test the performance of $t_{neg} = [0.5, 1.0, 1.5, 2.0, 4.0, 8.0]$ with a fixed $t_{pos} = 0.5$. Since the SR’s contrastive learning are relatively simple, larger temperatures can increase the learning efficiency. The results demonstrate that: within a certain range, the values of t_{pos} and t_{neg} have no significant influence on the experimental results.

Table 2. Comparison of different split size of mini-patches. All metrics are calculated on the DIV2K [1] validation set.

Size	1*1	2*2	3*3	4*4	8*8
↑ PSNR	27.30	26.93	26.78	26.65	26.48
↓ LPIPS	0.1722	0.1648	0.1643	0.1635	0.1596
↓ ICOO	27.43	27.21	27.14	26.82	26.65

Influence of different patch sizes. The patch size is also an important trade-off between the model performance and resource consumption; since the space complexity is $O(n^2)$. As illustrated in Table 2, we evaluated on EDSR [19] for $p = [1, 2, 3, 4, 8]$ on DIV2K [1]. To avoid the usage out of our GPU’s memory, we set the batch size to 16 especially. It is interesting that, within a certain range, the larger the patch size is, the better the perceptual quality. This phenomenon indicates that: the contrastive learning allows for more accurate mapping of similar HR details with smaller mini-patches, so as to achieve better performance on LPIPS.

Table 3. Comparisons with state-of-the-art methods. **Red** font denotes the best, and **blue** denotes the second best. DECLoss and DECLoss+ are trained on RRDB [36]. Specifically, DECLoss+ is a jointly training strategy that trains RRDB with DECLoss and RaGAN [36].

Benchmark	Metric	Bicubic	EDSR [19]	SRFlow [22]	RankSRGAN [41]	DECLoss	ESRGAN [36]	DECLoss+
DIV2K	↑ PSNR	24.11	28.97	27.06	26.55	28.47	26.64	27.01
	↓ LPIPS	0.210	0.138	0.103	0.099	0.118	0.092	0.090
	↓ ICOO	28.94	27.23	26.26	25.97	26.75	25.58	25.83
Urban100	↑ PSNR	21.70	24.51	23.69	22.98	24.70	22.78	23.27
	↓ LPIPS	0.237	0.140	0.116	0.122	0.113	0.108	0.105
	↓ ICOO	27.34	24.67	23.90	23.90	23.30	22.58	22.83
BSD100	↑ PSNR	24.65	26.24	24.67	24.13	25.54	23.97	24.24
	↓ LPIPS	0.198	0.158	0.115	0.114	0.138	0.108	0.106
	↓ ICOO	28.66	26.00	23.90	24.15	23.87	23.58	23.59
↓ GPU Hours		-	6.333	913.2	104.1	43.22	67.72	71.08

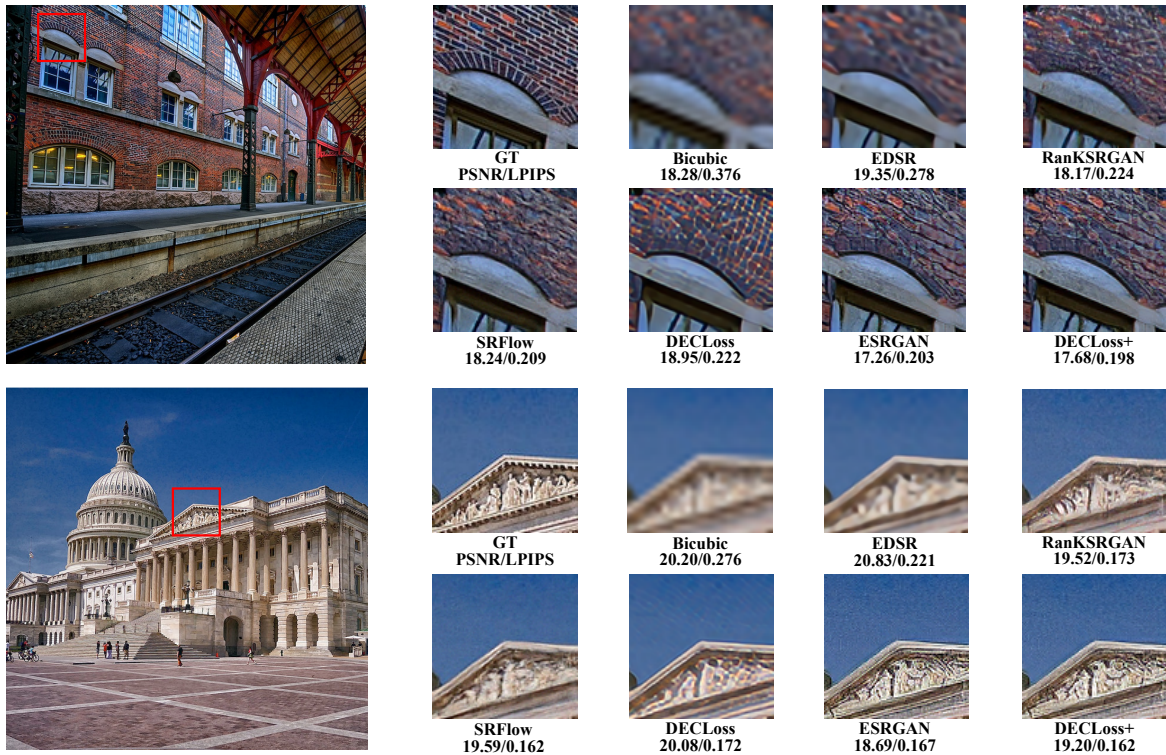


Figure 7. Comparisons with state-of-the-art methods. We compare POMs with GAN-based methods (RankSRGAN [41], ESRGAN [36] and ours). It is clearly that GAN-based methods outperform POMs in the perceptual quality. Our proposed DECLoss can generate more realistic textures among different categories.

5.4. Comparisons with State-of-the-art Methods

In addition to conducting the effectiveness of our DECLoss, we compared state-of-the-art methods. Note that, it is not necessary for our DECLoss to outperform the GAN-based method, our DECLoss required less GPU training time to achieve similar accuracy. Also in Table 3, our DECLoss, trained on RRDB, outperforms POMs. Compared with GAN-based methods: RankSRGAN [41] and ESRGAN [36], our DECLoss performed equivalently to RankSRGAN, with $2.4\times$ faster, and even DECLoss is 0.005

higher in LPIPS than ESRGAN on Urban100, as well as DECLoss achieved $1.57\times$ faster. We also show the orthogonality of our DECLoss, we apply RaGAN [36] with DECLoss on RRDB, denoted as DECLoss+, which outperformed a varieties of state-of-the-art methods. We illustrate these results in Fig. 7. Compared with a detail-enhanced SR model: SRFlow [22], DECLoss+ achieves 0.011 lower in LPIPS on Urban100, with $12.85\times$ faster.

6. Conclusion

In this work, we discovered two factors hindering the perceptual quality of PSNR-oriented models: the center-oriented optimization problem and low-frequency tendency. To better alleviate these problems, we proposed the Detail Enhanced Contrastive Loss (DECLOSS), consisting of the high-frequency enhanced module and spatial contrastive learning loss. Without any generate-adversarial processes, our DECLOSS achieved equivalent performance to GAN-based methods, but our method was $3.60\times$ faster. The Experimental results proved our method’s efficiency. It is also interesting to identify that (Table 2), the smaller patch size of the model can lead to the better the perceptual quality. However, due to the hardware memory constraints, the patch size cannot be reduced infinitely; thus, how to find this trade-off will be the key to our important future work.

References

- [1] Eirikur Agustsson and Radu Timofte. Ntire 2017 challenge on single image super-resolution: Dataset and study. In *The IEEE Conference on Computer Vision and Pattern Recognition (CVPR) Workshops*, July 2017. 6, 7
- [2] Namhyuk Ahn, Byungkoon Kang, and Kyung-Ah Sohn. Fast, accurate, and lightweight super-resolution with cascading residual network. In *Proceedings of the European Conference on Computer Vision (ECCV)*, pages 252–268, 2018. 2
- [3] Mathilde Caron, Ishan Misra, Julien Mairal, Priya Goyal, Piotr Bojanowski, and Armand Joulin. Unsupervised learning of visual features by contrasting cluster assignments. *arXiv preprint arXiv:2006.09882*, 2020. 3
- [4] Ting Chen, Simon Kornblith, Mohammad Norouzi, and Geoffrey Hinton. A simple framework for contrastive learning of visual representations. In *International Conference on Machine Learning*, pages 1597–1607. PMLR, 2020. 3, 5, 7
- [5] Chao Dong, Chen Change Loy, Kaiming He, and Xiaoou Tang. Image super-resolution using deep convolutional networks. *IEEE transactions on Pattern analysis and machine intelligence*, 38(2):295–307, 2015. 1, 2
- [6] Hayit Greenspan. Super-resolution in medical imaging. *The Computer Journal*, 52(1):43–63, 2009. 1
- [7] Jean-Bastien Grill, Florian Strub, Florent Altché, Corentin Tallec, Pierre H Richemond, Elena Buchatskaya, Carl Doersch, Bernardo Avila Pires, Zhaohan Daniel Guo, Mohammad Gheshlaghi Azar, et al. Bootstrap your own latent: A new approach to self-supervised learning. *arXiv preprint arXiv:2006.07733*, 2020. 3
- [8] Yong Guo, Jian Chen, Jingdong Wang, Qi Chen, Jiezhong Cao, Zeshuai Deng, Yanwu Xu, and Minghui Tan. Closed-loop matters: Dual regression networks for single image super-resolution. In *Proceedings of the IEEE/CVF Conference on Computer Vision and Pattern Recognition*, pages 5407–5416, 2020. 2
- [9] Kaiming He, Haoqi Fan, Yuxin Wu, Saining Xie, and Ross Girshick. Momentum contrast for unsupervised visual representation learning. In *Proceedings of the IEEE/CVF Conference on Computer Vision and Pattern Recognition*, pages 9729–9738, 2020. 3
- [10] Kaiming He, Xiangyu Zhang, Shaoqing Ren, and Jian Sun. Deep residual learning for image recognition. In *Proceedings of the IEEE Conference on Computer Vision and Pattern Recognition*, pages 770–778, 2016. 2
- [11] Jia-Bin Huang, Abhishek Singh, and Narendra Ahuja. Single image super-resolution from transformed self-exemplars. In *Proceedings of the IEEE Conference on Computer Vision and Pattern Recognition*, pages 5197–5206, 2015. 6, 7
- [12] Yawen Huang, Ling Shao, and Alejandro F Frangi. Simultaneous super-resolution and cross-modality synthesis of 3d medical images using weakly-supervised joint convolutional sparse coding. In *Proceedings of the IEEE Conference on Computer Vision and Pattern Recognition*, pages 6070–6079, 2017. 1
- [13] Justin Johnson, Alexandre Alahi, and Li Fei-Fei. Perceptual losses for real-time style transfer and super-resolution. In *European Conference on Computer Vision*, pages 694–711. Springer, 2016. 2, 5, 6
- [14] Jiwon Kim, Jung Kwon Lee, and Kyoung Mu Lee. Accurate image super-resolution using very deep convolutional networks. In *Proceedings of the IEEE Conference on Computer Vision and Pattern Recognition*, pages 1646–1654, 2016. 1, 2
- [15] Jiwon Kim, Jung Kwon Lee, and Kyoung Mu Lee. Deeply-recursive convolutional network for image super-resolution. In *Proceedings of the IEEE Conference on Computer Vision and Pattern Recognition*, pages 1637–1645, 2016. 2
- [16] Diederik P Kingma and Jimmy Ba. Adam: A method for stochastic optimization. *arXiv preprint arXiv:1412.6980*, 2014. 7
- [17] Christian Ledig, Lucas Theis, Ferenc Huszár, Jose Caballero, Andrew Cunningham, Alejandro Acosta, Andrew Aitken, Alykhan Tejani, Johannes Totz, Zehan Wang, et al. Photo-realistic single image super-resolution using a generative adversarial network. In *Proceedings of the IEEE Conference on Computer Vision and Pattern Recognition*, pages 4681–4690, 2017. 1, 2, 6
- [18] Wenbo Li, Kun Zhou, Lu Qi, Liying Lu, Nianjuan Jiang, Jiangbo Lu, and Jiaya Jia. Best-buddy gans for highly detailed image super-resolution. *arXiv preprint arXiv:2103.15295*, 2021. 2
- [19] Bee Lim, Sanghyun Son, Heewon Kim, Seungjun Nah, and Kyoung Mu Lee. Enhanced deep residual networks for single image super-resolution. In *Proceedings of the IEEE Conference on Computer Vision and Pattern Recognition Workshops*, pages 136–144, 2017. 1, 2, 6, 7, 8
- [20] Jie Liu, Wenjie Zhang, Yuting Tang, Jie Tang, and Gangshan Wu. Residual feature aggregation network for image super-resolution. In *Proceedings of the IEEE/CVF Conference on Computer Vision and Pattern Recognition*, pages 2359–2368, 2020. 2
- [21] Liying Lu, Wenbo Li, Xin Tao, Jiangbo Lu, and Jiaya Jia. Masa-sr: Matching acceleration and spatial adaptation for reference-based image super-resolution. In *Proceedings of the IEEE/CVF Conference on Computer Vision and Pattern Recognition*, pages 6368–6377, 2021. 2

- [22] Andreas Lugmayr, Martin Danelljan, Luc Van Gool, and Radu Timofte. Srflo: Learning the super-resolution space with normalizing flow. In *European Conference on Computer Vision*, pages 715–732. Springer, 2020. 8
- [23] Shunta Maeda. Unpaired image super-resolution using pseudo-supervision. In *Proceedings of the IEEE/CVF Conference on Computer Vision and Pattern Recognition*, pages 291–300, 2020. 2
- [24] David Martin, Charless Fowlkes, Doron Tal, and Jitendra Malik. A database of human segmented natural images and its application to evaluating segmentation algorithms and measuring ecological statistics. In *Proceedings Eighth IEEE International Conference on Computer Vision. ICCV 2001*, volume 2, pages 416–423. IEEE, 2001. 6
- [25] Aaron van den Oord, Yazhe Li, and Oriol Vinyals. Representation learning with contrastive predictive coding. *arXiv preprint arXiv:1807.03748*, 2018. 3
- [26] Oleg S Pinykh, Ksenia Pospelova, and Nick H Kamboj. Modeling human perception of image quality. *Journal of Digital Imaging*, 31(6):768–775, 2018. 2, 4
- [27] Pejman Rasti, Tonis Uiboupin, Sergio Escalera, and Gholamreza Anbarjafari. Convolutional neural network super resolution for face recognition in surveillance monitoring. In *International Conference on Articulated Motion and Deformable Objects*, pages 175–184. Springer, 2016. 1
- [28] Karen Simonyan and Andrew Zisserman. Very deep convolutional networks for large-scale image recognition. *arXiv preprint arXiv:1409.1556*, 2014. 6
- [29] Jae Woong Soh, Sunwoo Cho, and Nam Ik Cho. Meta-transfer learning for zero-shot super-resolution. In *Proceedings of the IEEE/CVF Conference on Computer Vision and Pattern Recognition*, pages 3516–3525, 2020. 2
- [30] Dehua Song, Yunhe Wang, Hanting Chen, Chang Xu, Chun-jing Xu, and DaCheng Tao. Addersr: Towards energy efficient image super-resolution. In *Proceedings of the IEEE/CVF Conference on Computer Vision and Pattern Recognition*, pages 15648–15657, 2021. 2
- [31] Baoli Sun, Xinchun Ye, Baopu Li, Haojie Li, Zhihui Wang, and Rui Xu. Learning scene structure guidance via cross-task knowledge transfer for single depth super-resolution. In *Proceedings of the IEEE/CVF Conference on Computer Vision and Pattern Recognition*, pages 7792–7801, 2021. 2
- [32] Ying Tai, Jian Yang, and Xiaoming Liu. Image super-resolution via deep recursive residual network. In *Proceedings of the IEEE Conference on Computer Vision and Pattern Recognition*, pages 3147–3155, 2017. 2
- [33] Laurens Van der Maaten and Geoffrey Hinton. Visualizing data using t-sne. *Journal of Machine Learning Research*, 9(1), 2008. 3
- [34] Longguang Wang, Yingqian Wang, Xiaoyu Dong, Qingyu Xu, Jungang Yang, Wei An, and Yulan Guo. Unsupervised degradation representation learning for blind super-resolution. In *Proceedings of the IEEE/CVF Conference on Computer Vision and Pattern Recognition*, pages 10581–10590, 2021. 3
- [35] Tongzhou Wang and Phillip Isola. Understanding contrastive representation learning through alignment and uniformity on the hypersphere. In *International Conference on Machine Learning*, pages 9929–9939. PMLR, 2020. 3
- [36] Xintao Wang, Ke Yu, Shixiang Wu, Jinjin Gu, Yihao Liu, Chao Dong, Yu Qiao, and Chen Change Loy. Esrgan: Enhanced super-resolution generative adversarial networks. In *Proceedings of the European Conference on Computer Vision (ECCV) workshops*, pages 0–0, 2018. 1, 2, 6, 7, 8
- [37] Yanbo Wang, Shaohui Lin, Yanyun Qu, Haiyan Wu, Zhizhong Zhang, Yuan Xie, and Angela Yao. Towards compact single image super-resolution via contrastive self-distillation. *arXiv preprint arXiv:2105.11683*, 2021. 3
- [38] Jiahui Zhang, Shijian Lu, Fangneng Zhan, and Yingchen Yu. Blind image super-resolution via contrastive representation learning. *arXiv preprint arXiv:2107.00708*, 2021. 3
- [39] Liangpei Zhang, Hongyan Zhang, Huanfeng Shen, and Pingxiang Li. A super-resolution reconstruction algorithm for surveillance images. *Signal Processing*, 90(3):848–859, 2010. 1
- [40] Richard Zhang, Phillip Isola, Alexei A Efros, Eli Shechtman, and Oliver Wang. The unreasonable effectiveness of deep features as a perceptual metric. In *Proceedings of the IEEE Conference on Computer Vision and Pattern Recognition*, pages 586–595, 2018. 2, 6
- [41] Wenlong Zhang, Yihao Liu, Chao Dong, and Yu Qiao. Rankrgan: Generative adversarial networks with ranker for image super-resolution. In *Proceedings of the IEEE/CVF International Conference on Computer Vision*, pages 3096–3105, 2019. 8
- [42] Yulun Zhang, Kunkeng Li, Kai Li, Lichen Wang, Bineng Zhong, and Yun Fu. Image super-resolution using very deep residual channel attention networks. In *ECCV*, 2018. 2
- [43] Yulun Zhang, Yapeng Tian, Yu Kong, Bineng Zhong, and Yun Fu. Residual dense network for image super-resolution. In *Proceedings of the IEEE Conference on Computer Vision and Pattern Recognition*, pages 2472–2481, 2018. 2